공학석사학위논문

Liquid Film Characteristics of Jet Impingement between Slit Injector and Wall

슬릿 인젝터와 벽과의 충돌 분무 액막 특성 연구

2018 년 2 월

서울대학교 대학원

기계항공공학부

이 형 원

슬릿 인젝터와 벽과의 충돌 분무 액막 특성 연구

Liquid Film Characteristics of Jet Impingement between Slit Injector and Wall

지도교수 윤 영 빈

이 논문을 공학석사 학위논문으로 제출함

2017 년 10 월

서울대학교 대학원

기계항공공학부

이 형 원

이형원의 공학석사 학위논문을 인준함

2017 년 12 월

위 원 장 _____

부위원장 _____

위 원 _____

Abstract

Liquid Film Characteristics of Jet Impingement between Slit Injector and Wall

Hyeongwon Lee
School of Mechanical and Aerospace Engineering
The Graduate School
Seoul National University

The liquid film generated by jet slit injector on the wall was analyzed by experimental approach. In rocket film cooling research, abundant studies on the perspective of heat transfer exist, but the study on hydrodynamic perspective, which investigates the interaction between slit jet and wall, is relatively less. Therefore, liquid film characteristics were investigated by measuring the liquid film thickness distribution in different experimental conditions. At first, the distribution was qualitatively analyzed by using back light imaging. Furthermore, quantitative measurement was performed by using liquid film

thickness sensor (fig. 1) based on electric conductance method, which had been designed and developed in the lab. Injection angle (15°, 30°, 45°), jet velocity (7m/s, 10.5m/s, 13.5m/s), and injection distance (45mm, 55mm, 65mm) were varied and the responses of the liquid film were observed. Having increased injection angle, mainstream thickness became thinner and the position of maximum film thickness moved upstream. Faster the jet velocity, wider the liquid film area and bigger the perturbation of the liquid film. The injection distance did not affect the characteristics of the liquid film considerably. Hydraulic jump effect was also observed and the large hydraulic jump affected the film thickness distribution of the mainstream. For advanced film cooling analysis, the result of this study can be applied to the development of rocket engine or thruster using the film cooling method.

Keywords: slit injector, liquid film thickness, high speed wire-mesh method, hydraulic jump effect

Student Number: 2016-20751

Contents

List of Tables

List of Figures

Chapter 1. INTRODUCTION

1.1 Film cooling for rocket engine

The cooling of the rocket engine uses mainly regenerative cooling and film cooling. Especially, the film cooling is a popular cooling method because of the small propellant flow rate in a small rocket engine and the small size of the combustion chamber. The schematics of film cooling mechanism is shown in Figure 1.1.

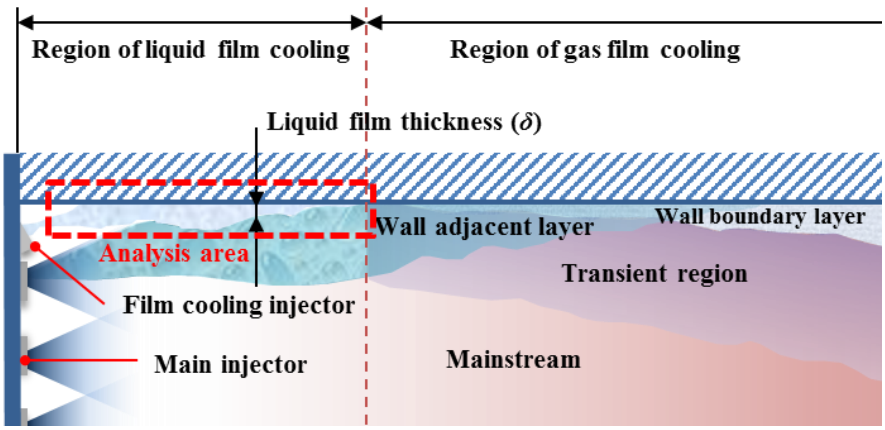

Figure 1.1 Schematics of film cooling mechanism

A mixing head which consists of main injector and a film cooling injector is on the left. The film cooling injector injects propellant directly onto the wall of the combustion chamber in the form of excess fuel or excess oxidant. The injected liquid film evaporates by the high temperature main stream. The evaporation protects the combustion chamber wall from the high temperature. In this way, cooling the engine combustion chamber wall using the evaporation is called film cooling.

This film cooling is important not only in the rocket engines but also in the gas turbine. The gas turbine industry studies high efficiency engines [1]. The Brighton cycle is essential in these studies explaining that the higher the turbine inlet temperature, the higher the efficiency. However, too high turbine inlet temperature provides a very harsh environment for the turbine blades. Therefore, the film cooling is the most traditional cooling method, so this method is also essential in the gas turbine.

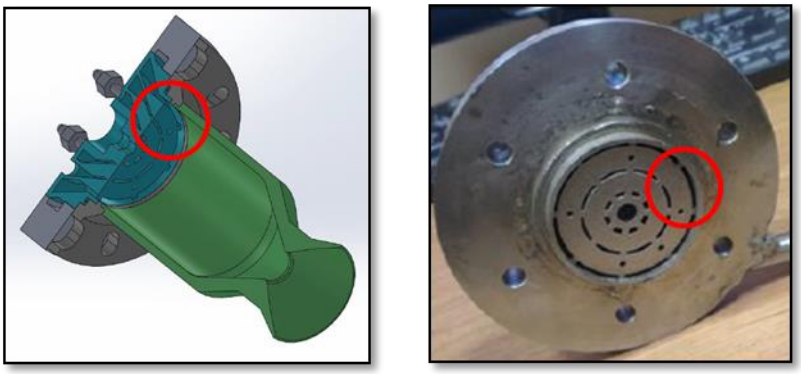

(a) DMT MAI-200-1 (200N GOX/kerosene engine)

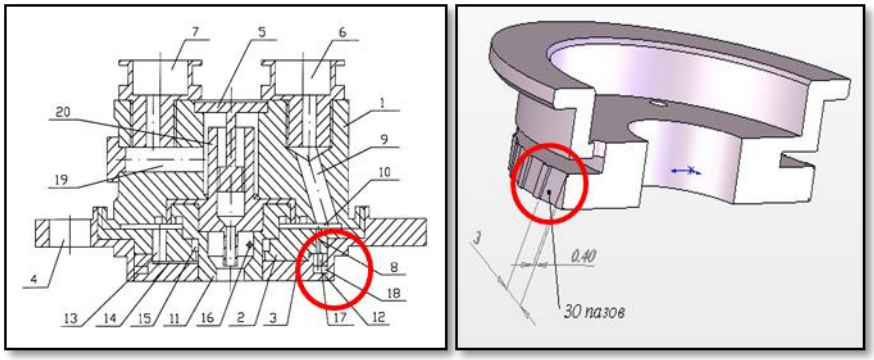

(b) MAI 200N GOX/GCH4 engine

Figure 1.2 Mixing heads for small rocket engine: (a) DMT MAI-200-1 (200N GOX/kerosene engine (ref. [2]), (b) MAI 200N GOX/GCH4 engine for research (ref. [3])

Rocket engine mixing heads using film cooling are shown in Figure 1.2. Aleksey G. Vorobyov's 200N GOX/kerosene engine is shown in Figure 1.2 (a). This engine has 30 slit injectors for film cooling. Dar'ya Y. Bogacheva's 200N GOX/GCH4 engine is shown in Figure 1.2 (b). This engine also has slit injectors for film cooling. In addition, when the main injector is an externally mixed coaxial swirl injector, there are two methods of colliding fuel and oxidant from the outside and of colliding with the wall without collision. The method of colliding with the wall without collision needs additional film cooling injector because it is directly combusted.

There are many researches for film cooling. The researches have a heat transfer perspective and a hydrodynamic perspective. It is usually hydro dynamically stable and is assumed to be ideal from the heat transfer perspective. However, it is neither stable nor ideal in real situation. Hydraulic analysis is inevitable for analyzing the real situation. Therefore, it is necessary to study the relationship between the slit injector and the combustion chamber wall. In this study, hydrodynamic analysis for film cooling has been performed.

1.2 Film thickness measurement methods

The propellant injected from the film cooling injector forms a liquid film on the wall of the combustion chamber. The most important parameter that governs the properties of the liquid film is the film thickness. Therefore, the liquid film thickness was measured to analyze the liquid film characteristics. As shown in Figure 1.3, there are various methods for measuring the liquid film thickness, including optical, ultrasonic, and electric conduction methods.

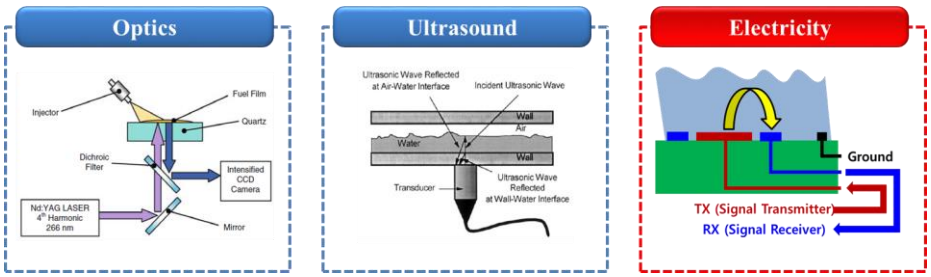

Figure 1.3 Various methods for measuring the liquid film thickness

The optical method has a high spatial resolution, but it has a disadvantage that there are errors due to diffraction and scattering. The ultrasonic method is a non-interference method, and has excellent time and spatial resolution, but it

is difficult to measure a thin liquid film thickness. The electric conduction method is a method of flowing electricity to the liquid film to obtain the thickness according to the magnitude of the voltage value. Among the various methods, this method has the advantages of high temporal resolution and low error rate. Because of the advantage of low rate to be the most important factor in the experiment, this thesis has been based on the electric conduction method.

1.3 Overview of present work

Many research has been conducted with film cooling and liquid film thickness measurement. Eldon L. Knuth et al. analyzed the mechanics of film cooling under the influence of high-velocity turbulent gas streams [4]. He determined the maximum allowable coolant flow rate for a stable coolant film. Richard Arnold et al. measured temperature gradients in axial and circumferential directions using LOX/CH4 subscale rocket combustion chamber [5]. He determined the influence between film-cooling efficiency and characteristics of slit injector. Takao Inamura et al. determined a numerical model that predicts the spray characteristics of a wall impingement injector [6]. He observed liquid film thickness on the wall by an automatic thickness measurement system. M. Damsohn and H. M. Prasser observed 2-dimensional liquid film thickness data using high speed wire-mesh method [7]. They analyzed ripple waves using continuous wavelet transform.

In summary, most studies are based on static characteristics. Hydrodynamic research for film cooling is unique. Therefore, in this study, based on the electric conduction method, the liquid film of the basic wall impingement

injection was analyzed.

1.4 Hydraulic jump effect

Hydraulic jump effect means that sudden flow velocity is slowed and the water level becomes high when a fast fluid enters a slow region. This mechanism is shown in Figure 1.4. As the flow transitions, the kinetic energy is rapidly changed to the potential energy, and the total energy is suddenly dropped due to the vortex flow and turbulence formed during the transition. This effect is also found in everyday life such as sinks.

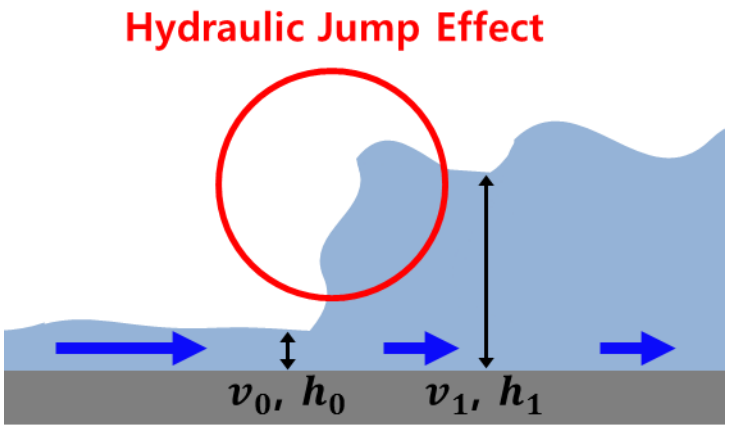

Figure 1.4 Schematics of hydraulic jump effect

This phenomenon develops as a mechanical energy conservation equation, and the conditions under which it is activated can be known :

$$\rho\left(gh_0 + \frac{1}{2}{v_0}^2\right) = \rho\left(gh_1 + \frac{1}{2}{v_1}^2\right) \qquad (1.1)$$

$$\frac{h_1}{h_0} = \frac{-1+\sqrt{1+\frac{8{v_0}^2}{gh_0}}}{2} \qquad (1.2)$$

Equation 1.3 shows the conditions for the expression of the hydraulic jump effect.

$$\frac{{v_0}^2}{gh_0} > 1, \quad \frac{h_1}{h_0} > 1 \qquad (1.3)$$

If the kinetic energy is larger than the potential energy, it can be seen that the hydraulic jump effect occurs. This effect has been mainly analyzed because this effect occurred entirely in this experiment.

Chapter 2. APPARATUS AND EXPERIMENTAL METHOD

2.1 Experimental apparatus

A schematics of injection experiment setup is shown in Figure 2.1. There are devices for analyzing a liquid film formed by a fluid ejected from a slit injector impinging a liquid film thickness measuring device. The fluid used in this experiment was 25-degree Celsius room temperature water, and the water was ejected on the liquid film thickness measuring device to analyze the two-dimensional distribution. This water is stored in the tank and then enters the injector through the differential pressure control system. The water flow rate was measured using a MFM (Mass Flow Meter). The MFM was an HP-228 turbine flow meter from Hoffer Flow Controls. The slit injector used in the experiment was a PC (polycarbonate)-made injector with an orifice of 4mm by 1mm.

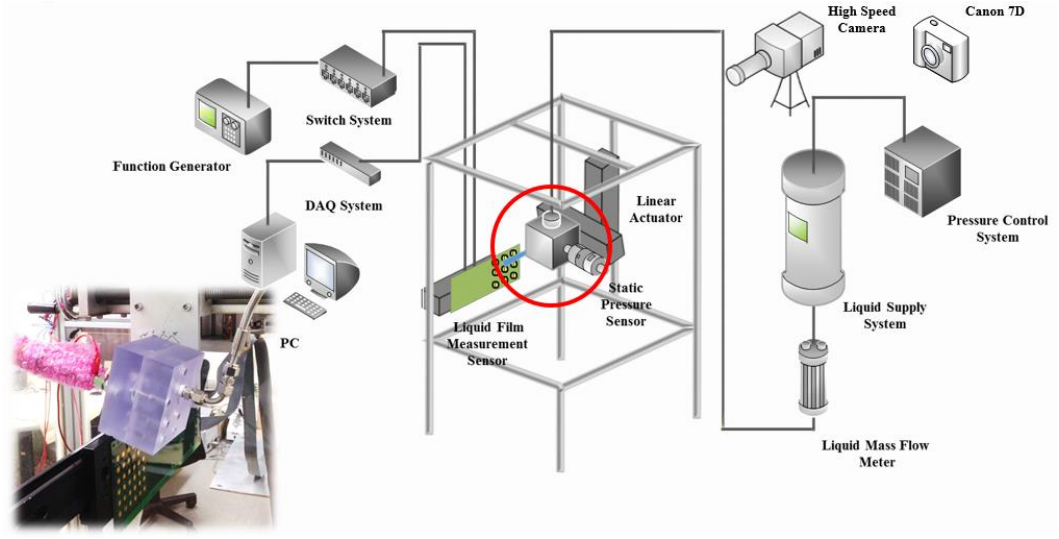

Figure 2.1 Schematics of injection experiment setup

The liquid film thickness measuring apparatus was based on the electric conduction method. A switch system for controlling the liquid film thickness measuring apparatus and the liquid film thickness measuring apparatus were manufactured in Cheilcad. The electric signal output to the liquid film thickness measuring device was outputted through the function generator. The function generator is EZ Digital's FG-7002C model. The electrical signal input from the liquid film thickness measuring device was a National Instrument's PCI-6133 DAQ. Valcom's static pressure sensor (capable of measuring 0-10bar) was used

to measure the static pressure of the injector internal manifold, and the National Instrument's USB-6218 BNC DAQ was used. In addition, to adjust the distance and angle between the injector and the wall, a three-dimensional linear actuator was installed to move the injector and film thickness measuring device.

At the time of liquid film image acquisition, the water was injected into a transparent quartz window instead of the film thickness measuring device to obtain an image. For average image acquisition, images were acquired at 1/50 sec using a Canon 7D camera and a 24-70mm lens. Also, high-speed camera Photron SA-5 was used for high-speed image acquisition.

2.2 Slit injector design

A slit injector to be used in the experiment was designed. As shown in Table 2.1, the mixing ratio, total propellant flow rate, total oxidizer flow rate, total film cooling injector flow rate, and film cooling injector number are substituted into the Ievlev's equation based on the LOX/GCH4 450N small engine design that our laboratory intends to develop by itself. The laboratory code was used to select film cooling injector specification.

LOX/GCH4 450N Small Engine Design	
3.5	**Mixing ratio (O/F)**
141.55 g/s	**Total propellant mass flow rate**
110.11 g/s	**Total oxidizer mass flow rate**
70.78 g/s	**Total film-cooling injector mass flow rate**
10	**A number of film-cooling injectors**

Table 2.1 LOX/GCH4 450N small engine design parameters

The total film cooling propellant flow rate was about 50% of the total propellant flow rate ejected. The reason for this is that in the Ph.D. thesis of Yulia S. Chudina [8]. It was stated that cooling flow rate was 50% of the total flow rate in the 200N methane engine. The design specification of the film cooling injector orifice were 1.2 mm wide and 0.3mm long. However, since the design specification was very small enough to comply with the manufacturing tolerances in the fabrication process, the scale-up design was performed about three times while maintaining the injection flow rate in order to reduce manufacturing errors. Accordingly, the scale-up design specification was 4mm wide and 1mm long in the orifice (Fig. 2.2).

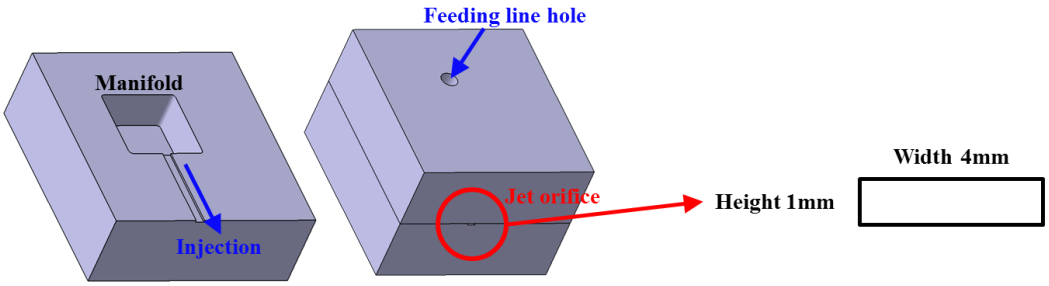

Figure 2.2 Slit injector geometry

In designing the jet injector, the orifice length was selected to be 40mm, so that the orifice length was larger than 1.5 in order to satisfy the condition that the flowmeter was sufficiently large. In order to observe the flow inside the injector, relatively strong and translucent PC (polycarbonate) was selected as the injector material. The feed line diameter for injecting water into the injector was also selected according to the flow rate injected by the injector.

2.3 Liquid film measurement sensor design

A liquid film thickness measurement device based on the electric conduction method was designed (Fig. 2.3). The measuring system consists of a liquid film thickness measurement board, a switch board and an RX board. The liquid film thickness measurement board is 300mm in width and 90mm in length and is composed of 36 cells.

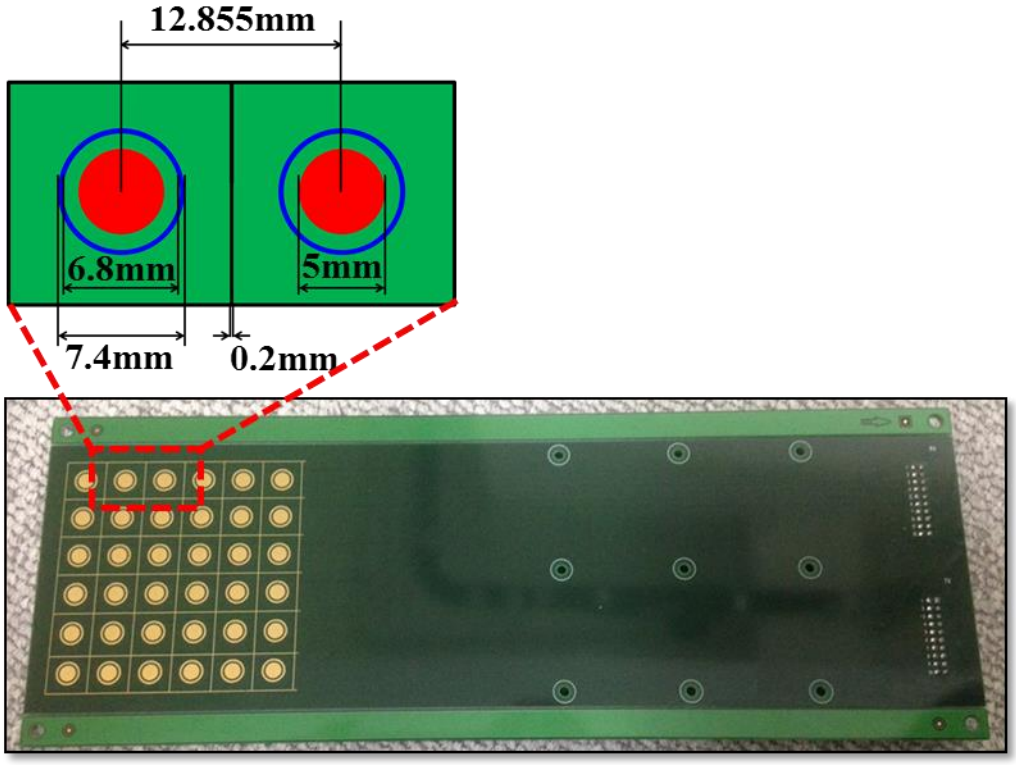

Figure 2.3 Liquid film thickness measurement board specification

The area to be measured is about 70mm, which is why the board is made so long to prevent water splashing on the connector. The measuring cell has a ring-shaped RX electrode with a diameter of 7.4mm on the outside, and a circular TX electrode with a diameter of 6.8mm (Fig. 2.3). The ring-shaped RX electrodes are bound together in rows, and the circular TX electrodes are bound together in columns (Fig. 2.4). A 0.2mm thick ground electrode was inserted between the cell and the cell to reduce the interference error signal between the cell and the cell.

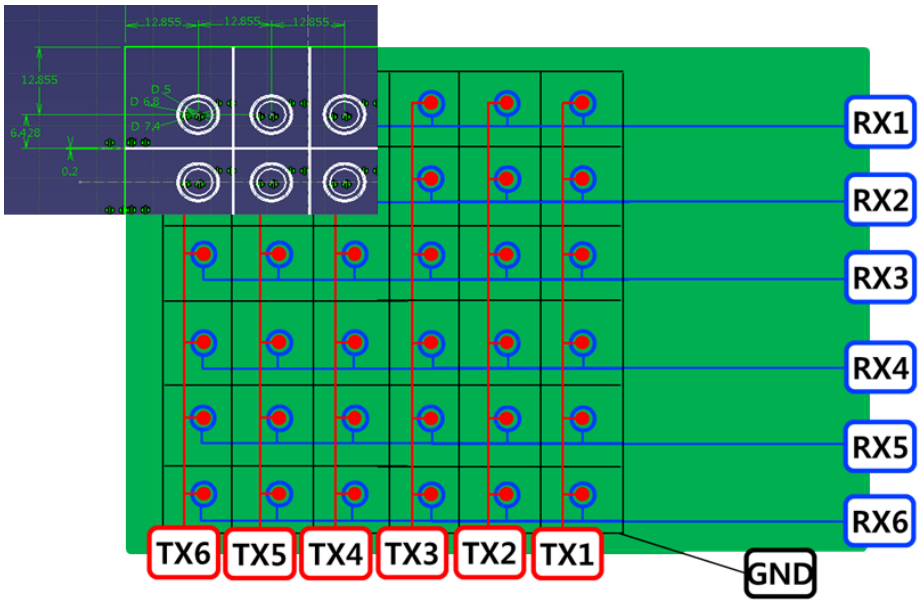

Figure 2.4 Schematics of liquid film thickness measurement board circuit

The switch board functions to sequentially output the output signal to the liquid film thickness measurement board. A detailed description of switch board will be given in the experimental method. The RX board converts the thickness signal input from the liquid film thickness measurement board into a BNC connector to transmit to the DAQ. In addition, the resistance value can be changed for each circuit on the RX board, so that the optimum liquid film thickness signal can be inputted. Cell optimization was performed through the COMSOL program to select the cell size, spacing, and number (Fig. 2.5). The liquid film thickness measurement range to be measured was about 0 to 1mm. Therefore, the optimum design was carried out to prevent saturation up to about 2mm.

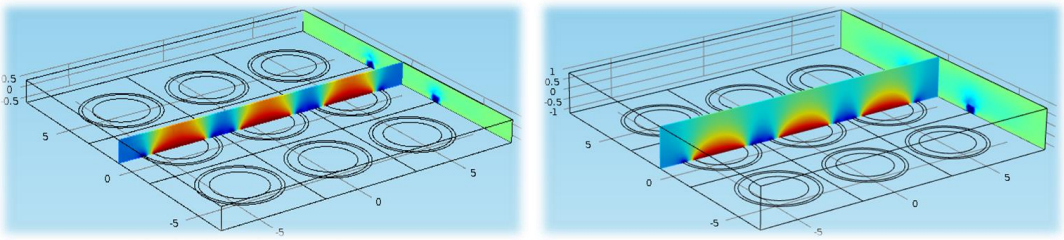

< Liquid film thickness 1.0mm >

< Liquid film thickness 2.0mm >

Figure 2.5 Cell optimization through the COMSOL program

The MATLAB code was applied to eliminate the delays that occur in the switching device itself when switching output signals. Since this delay was arbitrarily expressed, I developed and filtered the code that clears the signal caused by the delay itself, rather than filtering it to fit the sink. A code was developed to check the data to see if it was properly signaled and to verify that it worked properly every time the data was acquired. Finally, since data was stored in the midst of the sign signal output, data from the time when the signal was completely received was taken as the start of the storage.

2.4 Experimental methods

2.4.1 Image acquisition method

In order to obtain an image, a fluid was injected into a transparent quartz instead of the liquid film thickness measurement board. Averaged images and High speed images have been acquired (Fig. 2.6). The average images are images obtained by taking a picture at a speed of 1/50 sec with a Canon 7D camera and averaging a total of 50 pictures. Because the sensor analyzes the average liquid film thickness distribution over a 1 second period, the images also use a 1 second average image to analyze under the same conditions.

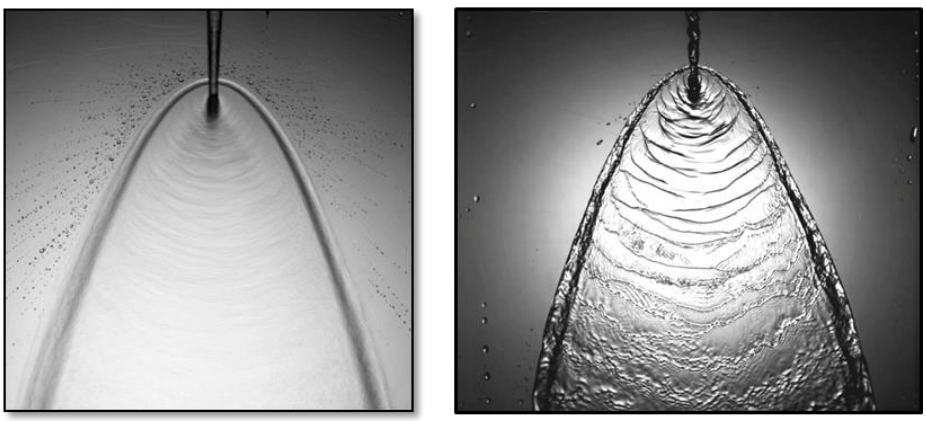

< Averaged image > **< High speed image >**

Figure 2.6 Averaged image and high speed image

Next, a High speed image was acquired to perform detailed liquid film foundation analysis. High speed images were acquired using Photron's SA-5 model. The image acquisition speed was set to 10,000 fps, and a monochrome image was obtained.

2.4.2 Sensor data acquisition method

A liquid film thickness measuring device was designed to quantitatively obtain a liquid film thickness distribution. The designed liquid film thickness measuring device was based on the electric conduction method. The electric conduction method is a method of outputting electricity to the formed liquid film to pass the fluid, and analyzing the electrical signal to measure the liquid film thickness (Fig. 2.7). The wire-mesh method is a method of quantitatively analyzing the two-dimensional liquid film thickness distribution by advancing the electric conduction method. However, the wire-mesh method has a measurement error due to interference between cells and cells. Therefore, the proposed method to reduce this error is the high-speed wire mesh method [7].

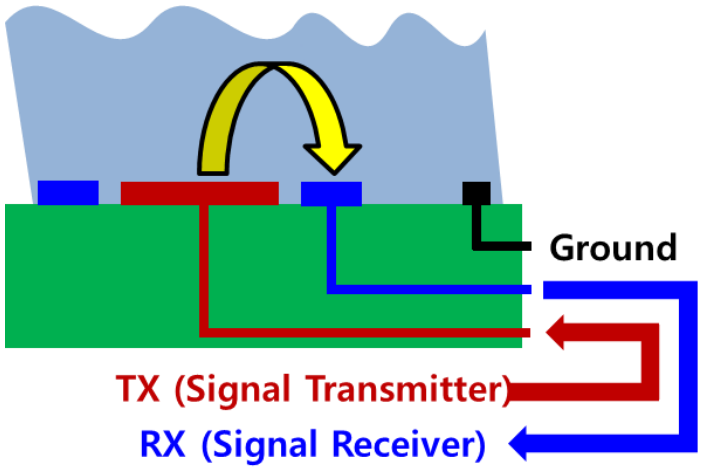

Figure 2.7 Mechanism of electric conductance method

As shown in Figure 2.8, there is a schematics of obtaining a liquid film thickness measuring device. At the bottom left, a signal is output via the function generator, and a given electrical signal is input to the DAQ through the liquid film thickness board via the switch device. The film thickness data acquired with DAQ was stored on a PC via Labview software from National Instruments. In the first sequence, the switch device will output electrical signals in only first column. So DAQ only receives data about first column. The second sequence then outputs the electrical signal in only second column.

So this time, DAQ only receives data about second column. In this way, when the data is received at high speed, the entire area can be acquired in a short time. The reason for using this method is that there is a merit that interference effect between cells is reduced, and circuit diagram is also simplified. In addition, the electric signal should be outputted as AC, not DC. The reason is that when voltage is applied to water by DC, electrolysis occurs. When electrolysis occurs, water molecules are split, which can increase the measurement error and destroy the sensor [9].

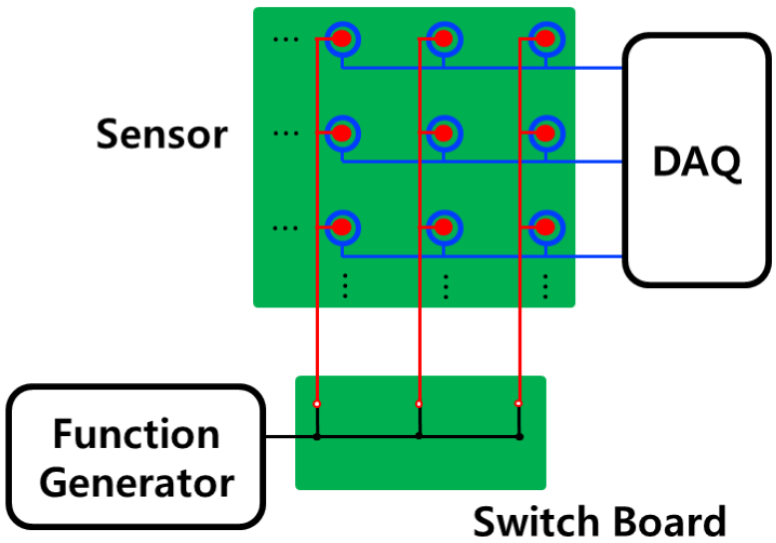

Figure 2.8 Schematics of obtaining a liquid film thickness measuring device

Acquisition speed was selected for high-speed data acquisition. The sine wave signal output from the function generator was selected at 10 kHz, and the switching speed of the switching device was also selected at 10 kHz so that the signal was switched every cycle. The sampling rate was chosen to be 1 MHz, and approximately 100 samples were sampled in one sinusoidal wave to reduce the measurement error. Based on this measurement rate, the speed at which a 6 × 6 data was once taken over the entire area was controlled to be about 1.6 kHz. So the average value of about 1666 data was used in one second. The spatial resolution was improved because the 6x6 spatial resolution of 36 cells was too low to analyze the film thickness distribution. Assuming that the injected fluid is steady state, the 12x12 spatial resolution is increased by moving the board to be measured to four positions. The 6x6 spatial resolution spacing is about 13mm, with a 12x12 spatial resolution spacing of about 6.5mm, which is about twice the resolution. At this time, since the diameter of the cell was 7.5 mm and the interval was 5.5 mm, the overlapping area of the cells occurred and the overlapping area of about 17% occurred. However, this method was adopted because 12x12 data was more qualitatively and quantitatively closer to the

actual liquid film distribution than simply 6x6 data.

2.5 Experimental condition

As shown in Figure 2.9, there are actual injection test photograph and schematics. As shown in the figure, experimental conditions such as injection angle, injection speed, and injection distance were selected. The experimental range according to the experimental condition was selected as shown in the Table 2.2. Each range was selected based on the NASA report [10]. According to the NASA report, liquid film cooling injection angles should be between about 25 and 35 degrees Celsius, and 30 to 40 percent of the propellant flow rate is used for film cooling. In addition, to generalize the experimental data, injection speed was dimensionless by jet Reynolds number and jetting distance was dimensionless by non-dimensional distance. However, for ease of analysis, out of the forthcoming results, the results are summarized in a more understandable m / s.

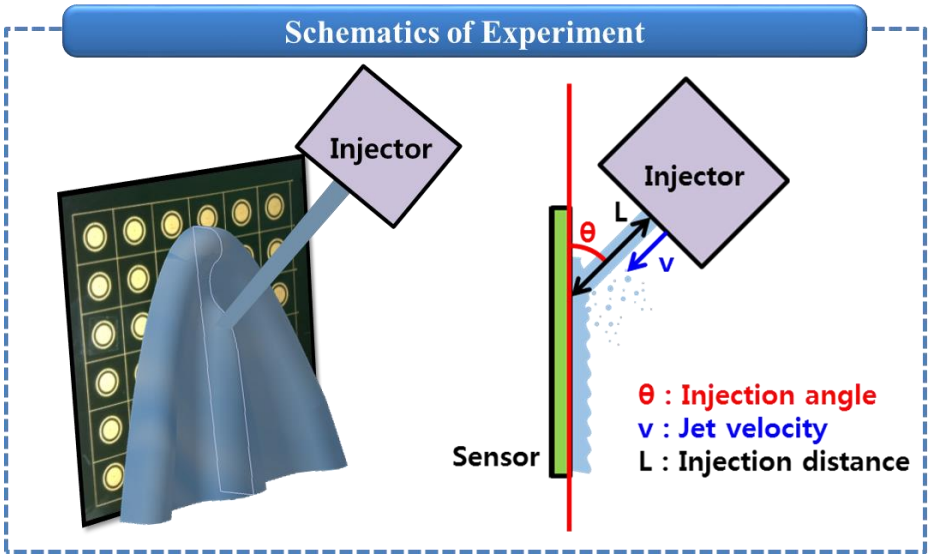

Figure 2.9 Schematics of injection test

Notation	Range	Parameter
θ	15 / 30 / 45 [1]	Injection angle [°]
Re_j	12,400 / 18,600 / 23,900 [1]	Jet Reynolds number [ ]
v	7 / 10.5 / 13.5	Jet velocity [m/s]
L*	45 / 55 / 65	Dimensionless injection distance [ ]

Table 2.2 Experimental range

Chapter 3. RESULTS AND DISCUSSTION

3.1 Basic characteristics of slit injector

At first, the basic injection of the slit injector was briefly analyzed. The basic injection characteristics of the slit injector were injected in the form of an orifice immediately after the outlet, but after a certain distance, the flow was observed to converge to one point (Fig. 3.1). This concentrated flow had the characteristic of entering the expanding area again. This basic characteristic is observed not only in the previous research [11] but also in the injector used in this study, which is qualitatively expressed in the low-speed region, but observed that the turbulent flow becomes strong and dulled at the rate of 13.5 m / s.

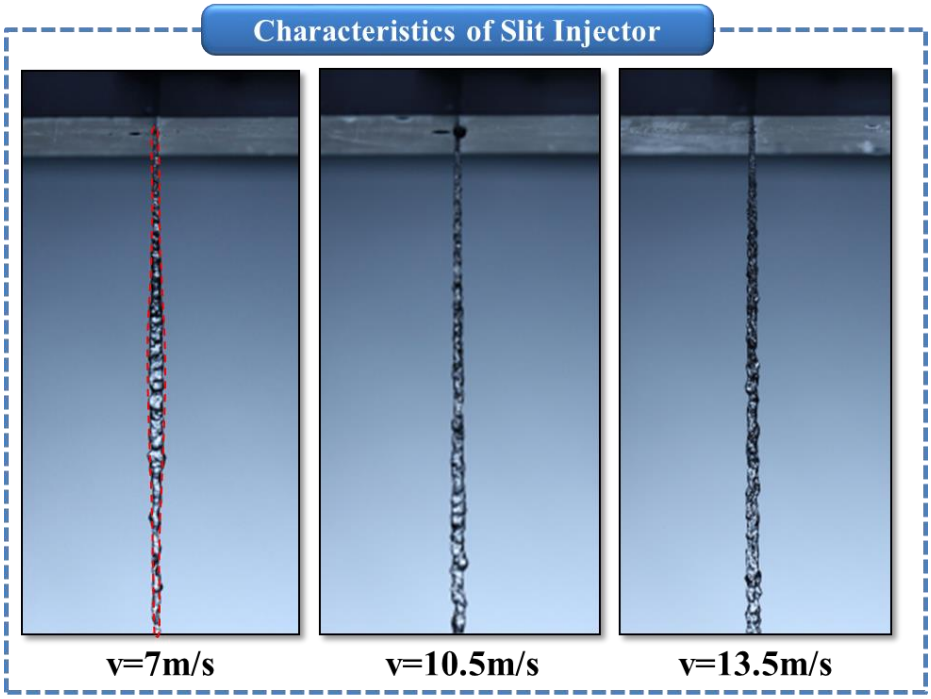

Figure 3.1 Injection characteristics of slit injector according to injection speed

3.2 Sensor calibration and verification

3.2.1 Sensor calibration

In the electrical conduction method, the liquid film thickness is obtained through the measured voltage value. So, it is necessary to know the liquid film thickness value appropriate for each voltage value. This is called calibration. Calibration methods used in the electrical conduction method include a method of forming a thickness by sandwiching between flat plates, and a method of turning a thick roller to a sensor. Among them, the roller method consumes a lot of manufacturing cost because the roller of each thickness to be calibrated is separately required [12]. However, the sandwich method is advantageous in that it can calibrate various thicknesses using a single calibrating device since the thickness is formed using a thickness gauge and the plate is fixed. Therefore, the sandwich type calibration was performed in this study.

Thus, the calibration range was from 0.05mm to 1mm, and the calibration was divided into 11 total. Since the optimized liquid film thickness measuring device saturates the voltage value at about 2 mm, the area where the actual data analysis is performed can acquire the data in a curve where the curve is

sufficiently steep. The 11 data thus obtained were drawn with a quadratic linear function as a calibration curve. The reason for this is that the trend line value of the curve fitting constant R^2 is closest to the fourth order linear function.

A total of thirty-six cells existed on the liquid film thickness measurement board, and one cell was designated as a reference cell since it was necessary to determine the stored data.

Since this reference cell had to catch the reference, the cell was closed with a scotch tape to prevent electricity from flowing. Only the remaining 35 cells were independently calibrated independently to reduce the data acquisition error of each cell. The actual reference cell was the cell located at TX6, RX3, and the calibration curve of this cell came from the curve of TX6, RX4 next to it. At this time, the process of confirming the error of the calibration curve with each other was performed, and since the error was less than 2% (Fig. 3.2), it was judged that it would be reasonable to adopt this method. As shown in Fig. 3.3, the liquid film thickness measurement error was less than about 3% through about 1600 data acquisitions.

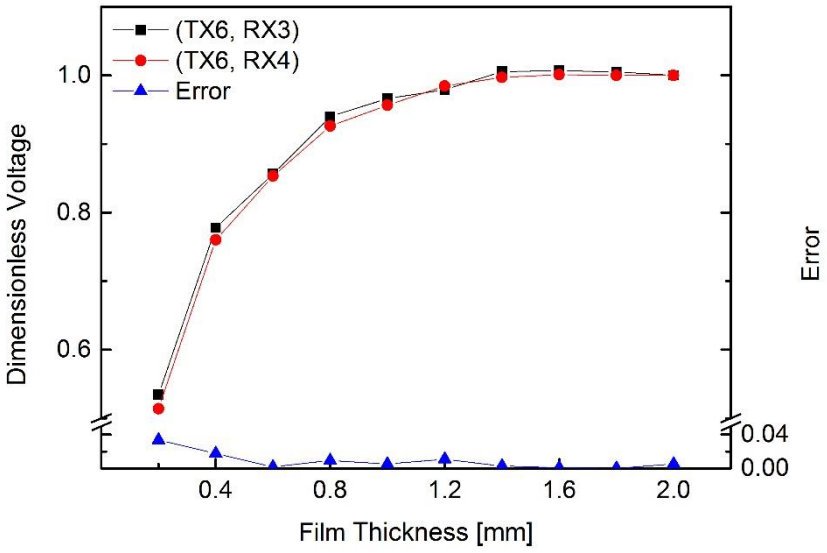

Figure 3.2 Calibration comparison with (TX6, RX3) and (TX6, RX4)

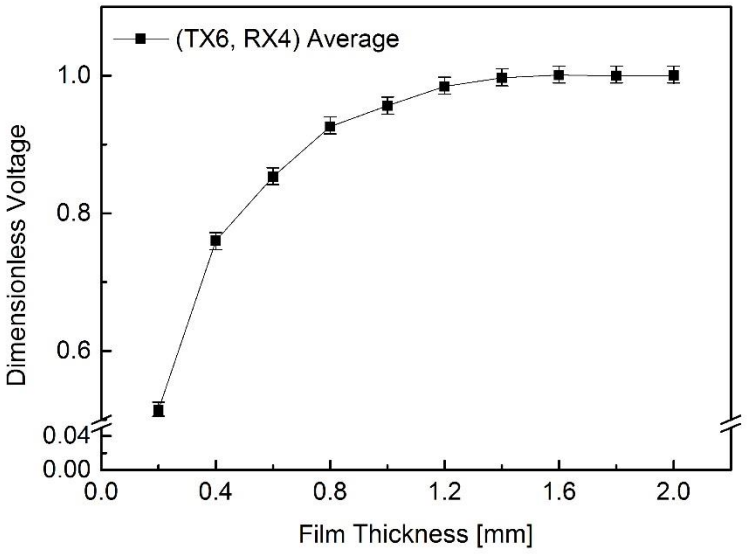

Figure 3.3 Average calibration graph

3.2.2 Sensor verification

Prior to quantitative analysis, a liquid film thickness measurement device was verified. Comparisons with previous research results and comparative analysis with actual injection images were conducted for verification. The reason for this is that it is difficult to measure accuracy because there is no perfect film thickness measuring device in these days [6].

This is a comparison with previous research results. Figure 3.4 is a schematic view of the liquid film formed on the sensor. For quantitative analysis, coordinate selection was performed first. The origin of the point of impact, the x-axis in the radial direction, the y-axis in the direction in which the fluid flows, and the z-axis in the direction in which the liquid film thickness is formed. Accordingly, the cross-sectional thicknesses y = 6mm, 18mm, and 30mm were experimentally obtained and plotted graphically. In order to compare these experimental data (Fig. 3.5 (b)), we compared it with previous numerical analysis data graph (Fig. 3.5 (a)) [6]. The two results show a similar tendency that the three large peaks become dull as y increases and the thickness around the impact area becomes rather thick, so that the overall thickness value

becomes flat. This tendency shows that the thickness tendency is consistent with the previous study.

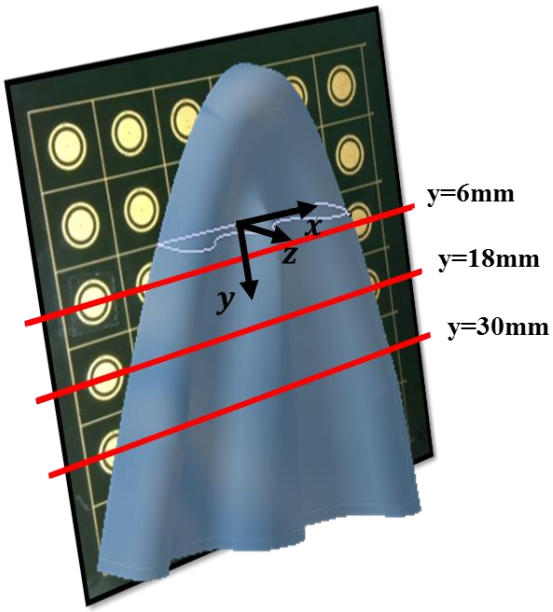

Figure 3.4 Selection of coordinate system

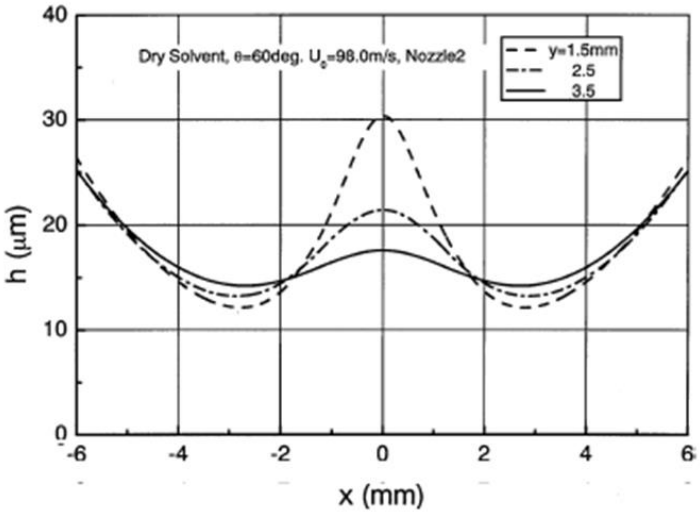

< Numerical Analysis (T. Inamura et al.[6]) >

Figure 3.5 (a) Numerical analysis of previous study

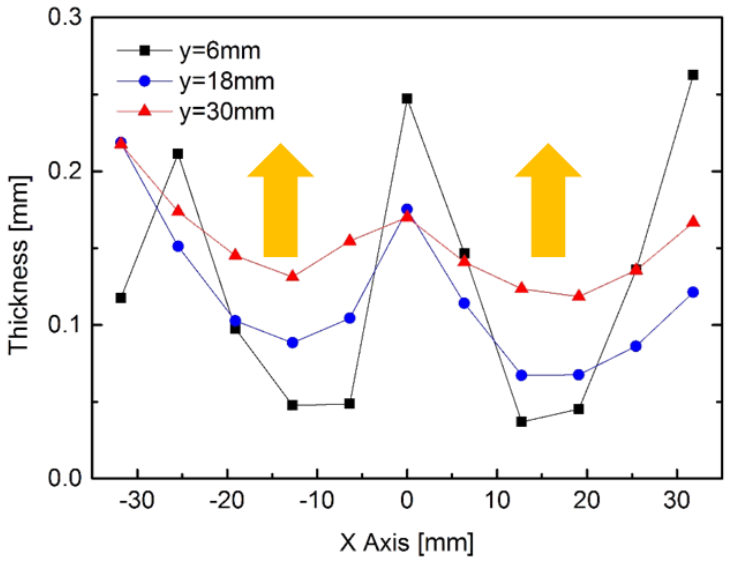

< Experimental Analysis (θ=30° v=13.5m/s L=55) >

Figure 3.5 (b) Experimental analysis of this study

Next, a comparison analysis was performed between the injection image and the sensor data. In the figure 3.6, the image shown on the left is a back light image, and the image on the right is a two-dimensional plots of the sensor data. First, the image on the left and the sensor data on the right did not match exactly. The reason for this is the spatial resolution problem, which is an inherent limitation of the electric conduction method. However, as the fluid descends downstream, fully improves and senses in the downstream region. Another reason is the perturbation of the liquid film flow itself. This problem was mentioned in the previous study [6] and it was injected to see the static characteristics, but the larger the jetting rate due to the droplet generation after the collision, the larger the perturbation. This perturbation averaged the data acquired for a second, but decided that it affected. There was this spatial resolution problem, but there was also the advantage of the sensor. The sensor is relatively accurate in liquid film thickness. As shown Figure 3.6, it is not possible to judge the thickness of the liquid film as the image, but it was able to clearly determine how the liquid film thickness was formed with the sensor data. Based on this, the change of the liquid film thickness distribution in the radial direction and the change in the liquid film thickness distribution in the

axial direction were compared and analyzed.

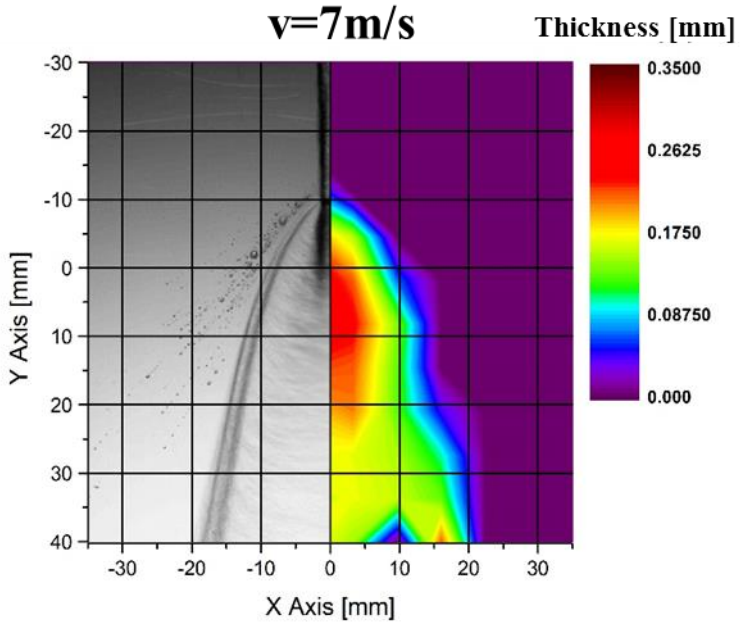

Figure 3.6 (a) Liquid film thickness distribution (θ=15˚, v=7m/s, L*=45)

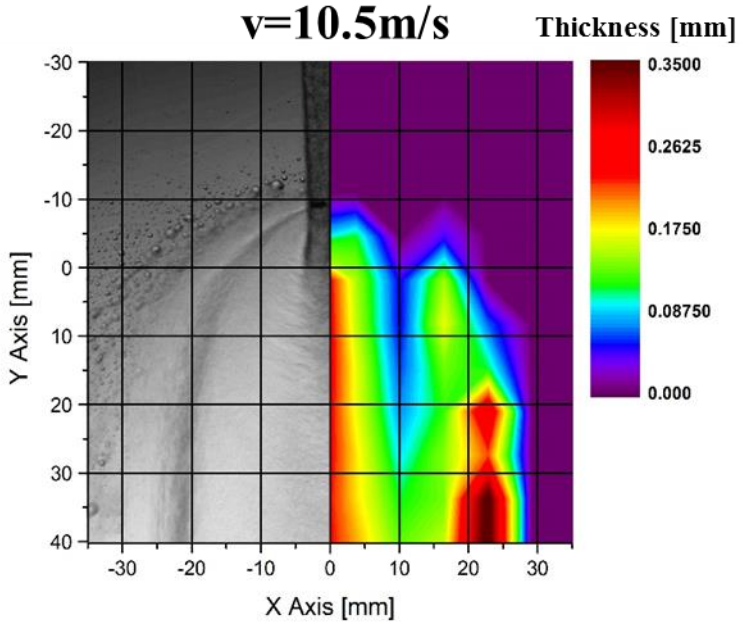

Figure 3.6 (b) Liquid film thickness distribution (θ=15˚, v=10.5m/s, L*=45)

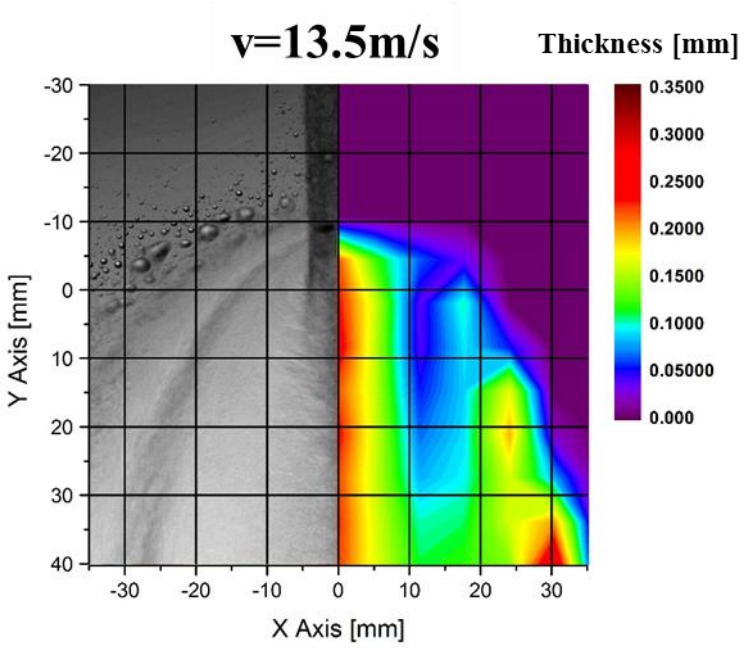

Figure 3.6 (c) Liquid film thickness distribution (θ=15˚, v=13.5m/s, L*=45)

3.3 Basic analysis of liquid film

Before the detailed results of the axial direction and the radial direction were observed, a basic analysis was performed on the liquid film formed after the wall collision injection. Figure 3.7 is an high speed image obtained under the condition of θ=30° , v=7m/s, L*=45. This image describes the mechanism and characteristics of the basic collision spray.

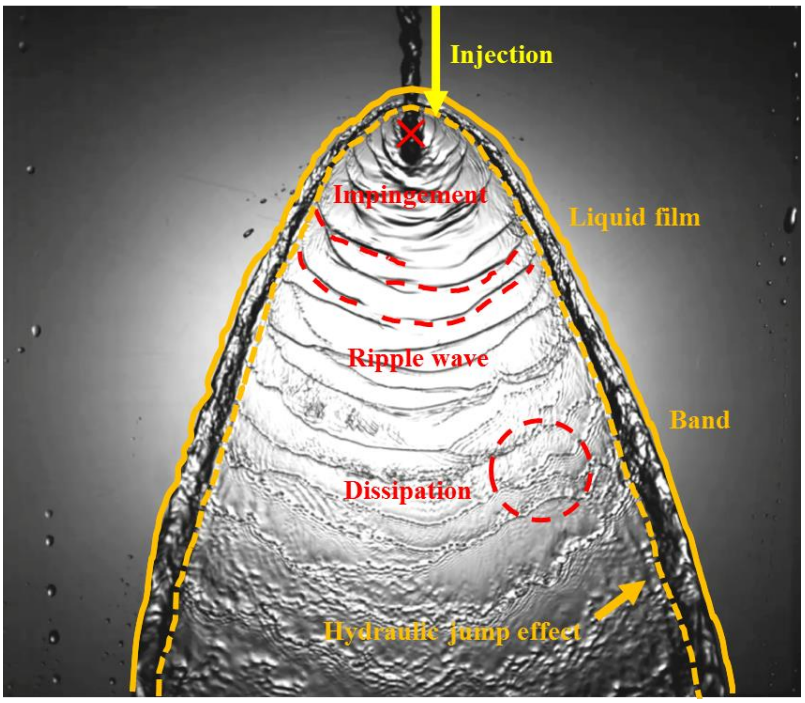

< Experimental condition θ=30°, v=7m/s, L*=45 >

Figure 3.7 Characteristics and mechanism of impinging liquid film

First, the mechanism of collision injection is divided into three major parts. The three were injection, collision and parabolic liquid film formation. There are two main characteristics of the liquid film. First, a ripple wave was created in the liquid film. Because the experimental conditions are fixed, a small wave with a relatively constant period is generated. The small waves thus generated were dissipated downstream by friction with the wall surface.

Second, it can be confirmed that a thick band is formed on the outer surface of the liquid film. This thick band was created by the sudden increase in water level caused by the hydraulic jump described above. As the jet fluid hits the wall and spreads, the flow velocity is slowed, and suddenly the water level suddenly increases and the flow velocity rapidly decreases. It can be seen that the thick band is formed by the surface tension while the velocity converges to zero by the friction.

In addition, as shown in figure 3.7, the upstream band is thinner than the downstream. The reason for this is that at the upstream side, the velocity converges to 0 faster due to gravity and friction, while the thicker band is formed as the gravity accelerates toward the downstream. Based on these basic collision spray characteristics, qualitative analysis and quantitative analysis

were carried out.

3.4 Qualitative characteristics

In order to perform a qualitative analysis, the 1-second average photograph was analyzed to understand the overall tendency. Two of the experimental conditions were fixed as dependent variables, and only one of them was replaced by an independent variable.

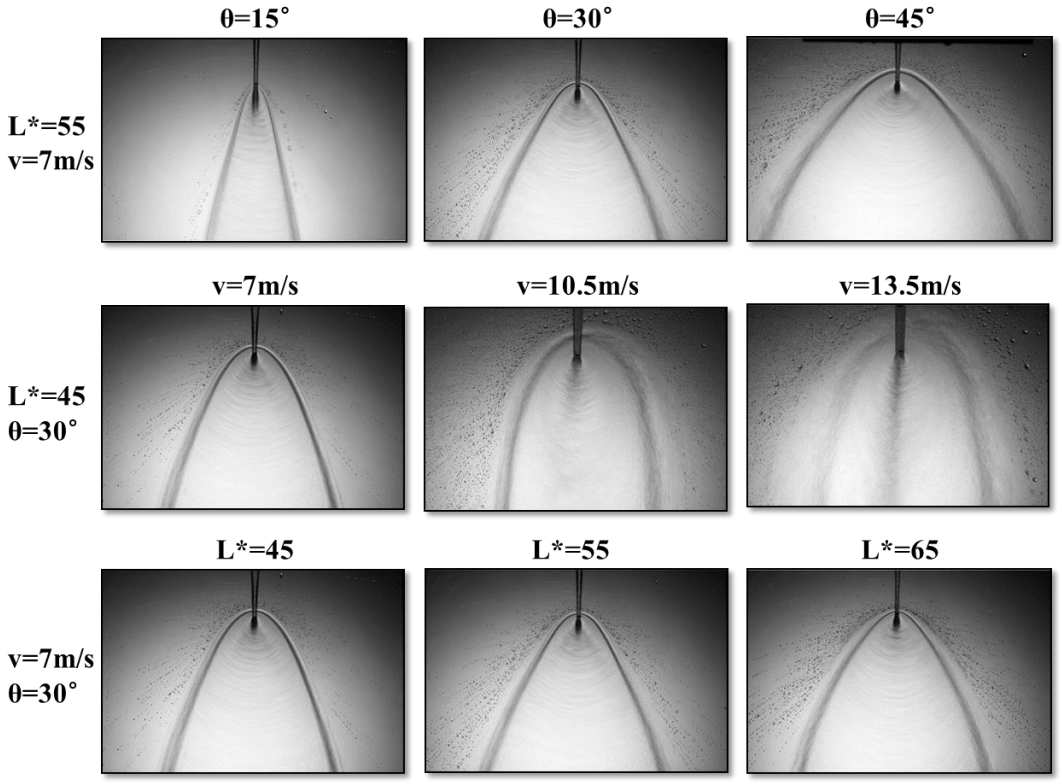

Figure 3.8 1-second average photograph of various conditions

As shown in figure 3.8, it was found that the liquid film area increases as the injection angle increases. As the jet speed increases, the band appearing on the outside of the liquid film becomes blurred (Fig. 3.8). This means that the liquid perturbation increases as the injection rate increases. It was confirmed that the liquid film shape was not greatly influenced by the ejection distance.

3.5 Quantitative characteristics

3.5.1 Film thickness characteristics of radial direction

In the coordinate system, the change in the thickness distribution of the x-axis was analyzed because the injection impact point is the origin and now it is the radial thickness distribution change. The distribution of injection angle, injection velocity, and injection angle were investigated. At the downstream (y = 40mm) of the liquid film cross section, the fluid became fully development. As shown in Figure 3.9, there were two characteristics. First, as the jet angle increases, the thickness of the main flow decreases. Second, as the spray angle increases, the thickness of the outer wall becomes thinner, which means that the hydraulic jump effect is weakened. These two features analyze that when the injection angle is low, most of the injected fluid flows downward as it is, but the flow is reversed to the left or right as the injection angle increases.

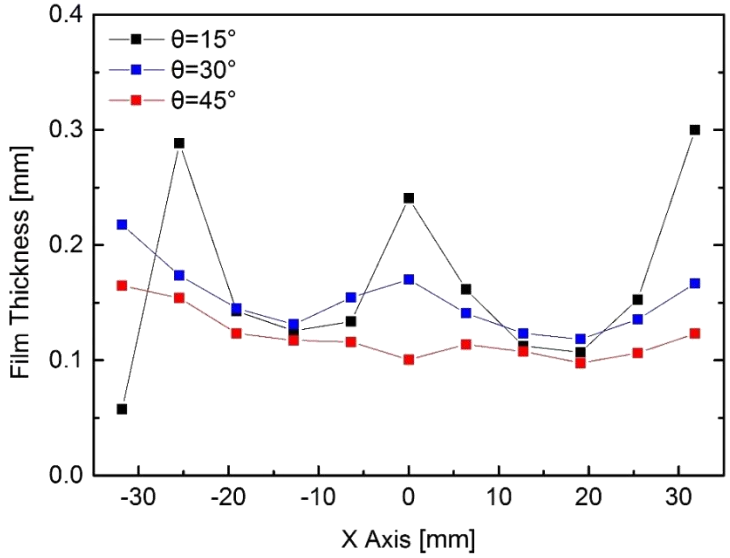

Figure 3.9 Radial film thickness depending on angle (v=13.5m/s, L*=45, y=40mm)

Next is the x axis thickness change with the injection speed (Fig. 3.10). The larger injection speed means that the injection flow rate becomes larger because the injection area is already fixed. Therefore, it can be confirmed that the thickness of the main flow is thickened as the injection flow rate increases, and that the area of the liquid film injected increases as the injection flow rate increases. The reason for these two characteristics is that, at high speeds, unlike in the low speed range, the flow rate increases and the fluid to the downstream

increases, and the fluid to the left or the upstream increases.

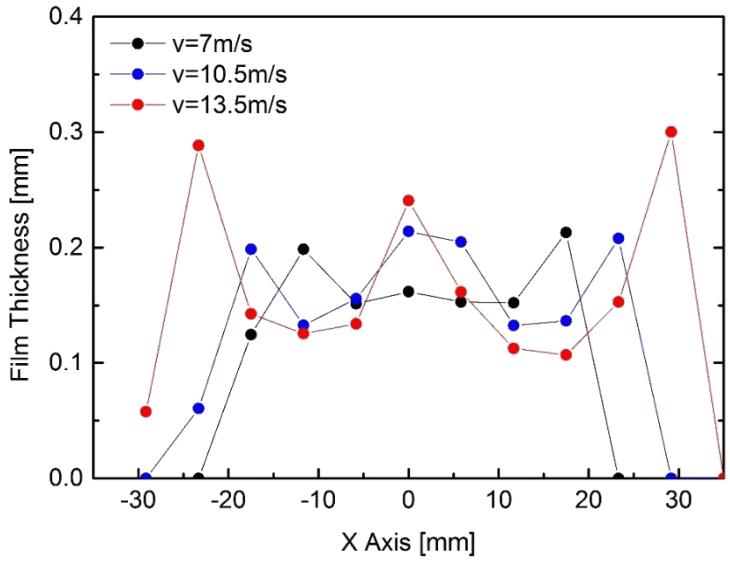

Figure 3.10 Radial film thickness depending on jet speed (θ=15° , L*=55, y=40mm)

Next, we checked the thickness variation of the x-axis according to the injection distance between the injector and the wall (Fig. 3.11). In the case of the ejection distance, as mentioned in the back light image analysis, the quantitative data also did not show a large change according to the ejection

distance. In addition, it can be seen that there is a slight measurement error only in L = 65 cases. This error is analyzed as a spatial error due to the size of the cell itself and the size of the cell itself.

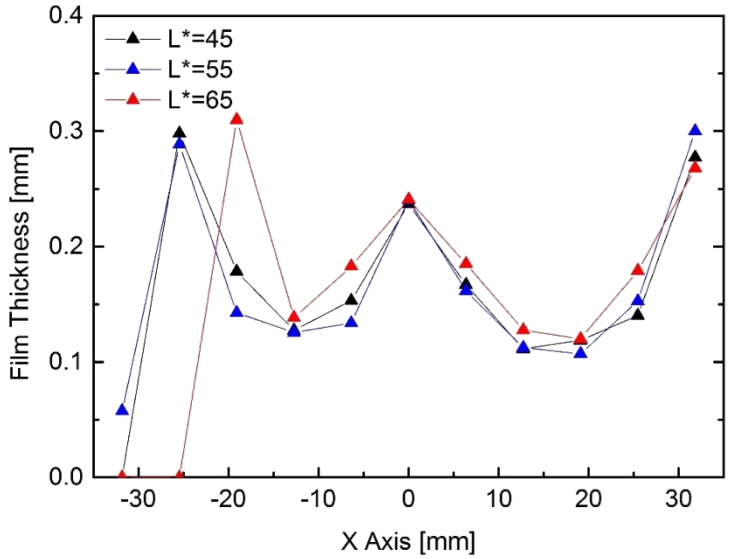

Figure 3.11 Radial film thickness depending on jet distance (θ=15° , v=13.5m/s, y=40mm)

3.5.2 Film thickness characteristics of axial direction

So far, the change in the thickness distribution of the x-axis has been analyzed, but now the change in the thickness distribution of the y-axis, that is, the section cut in the longitudinal direction, has been analyzed. As shown in Figure 3.12, it is easy to understand if you think that the section is laid in the graph.

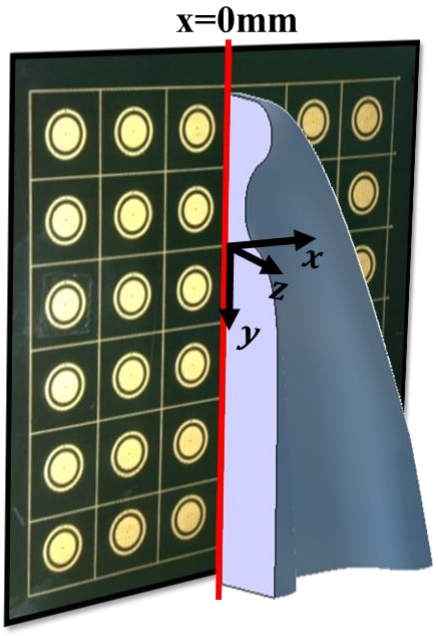

Figure 3.12 Axial direction film thickness distribution

First, the y-axis thickness distribution changes with the injection angle (Fig. 3.13). First, as the angle increases, the position of the highest thickness shifts to the upstream. This phenomenon is also analyzed when the angle is low, while the flow flows directly to the downstream side, while the reverse flow in the radial direction or the upstream direction occurs as the angle increases, and the maximum thickness moves upstream.

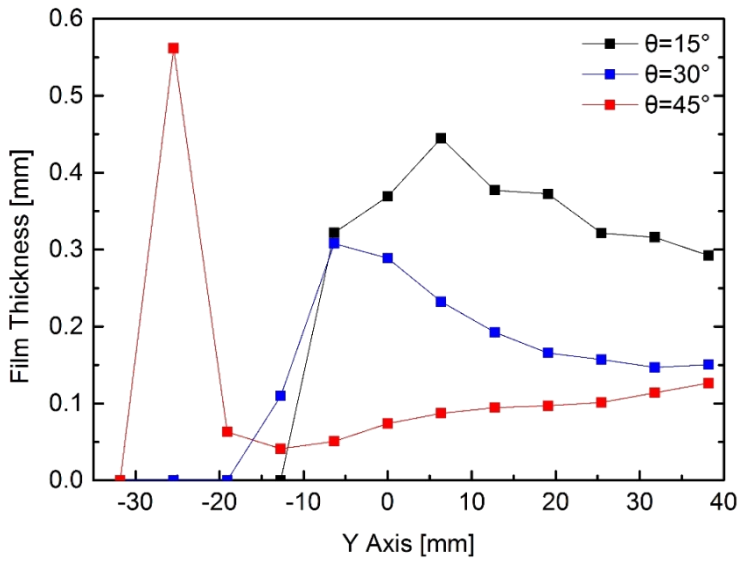

Figure 3.13 Axial film thickness depending on angle (v=10.5m/s, L*=55, x=0mm)

Also, the 15 and 30 degree cases gradually decreased in thickness toward the downstream, but the 45 degree cases tend to gradually increase in thickness. This trend suggests that a relatively thick hydraulic jump occurred upstream in the 45 degree case and that a large hydraulic jump upstream would create a tendency to increase thickness in the mainstream. In other words, it was concluded that the hydraulic jump phenomenon had a great influence on the film thickness.

In the same way, the y-axis thickness distribution according to the injection speed was analyzed (Fig. 3.14). Unlike in the analysis so far, it has been difficult to judge the propensity to change the jet speed in three cases. Therefore, additional cases were experimented and analyzed. A total of seven cases were tested, and the most downstream thickness of the analysis side was redrawn with a graph for each jet speed (Fig. 3.15).

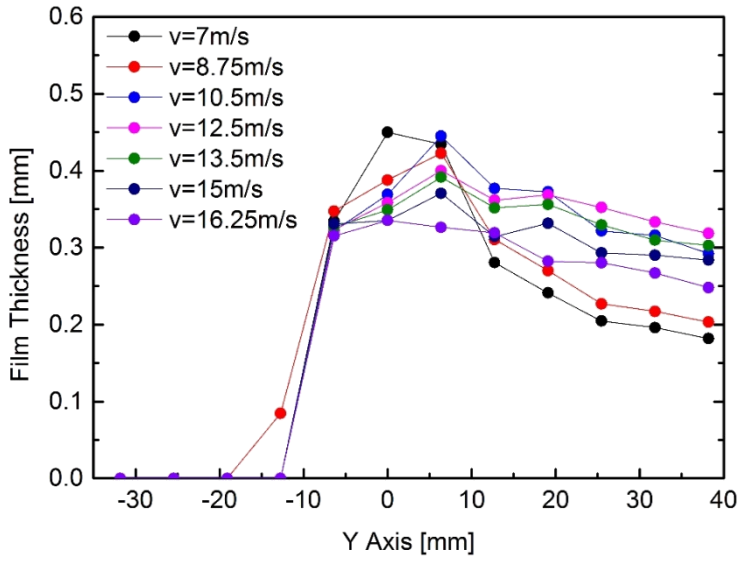

Figure 3.14 Axial film thickness depending on jet speed (θ=15° , L*=55, x=0mm)

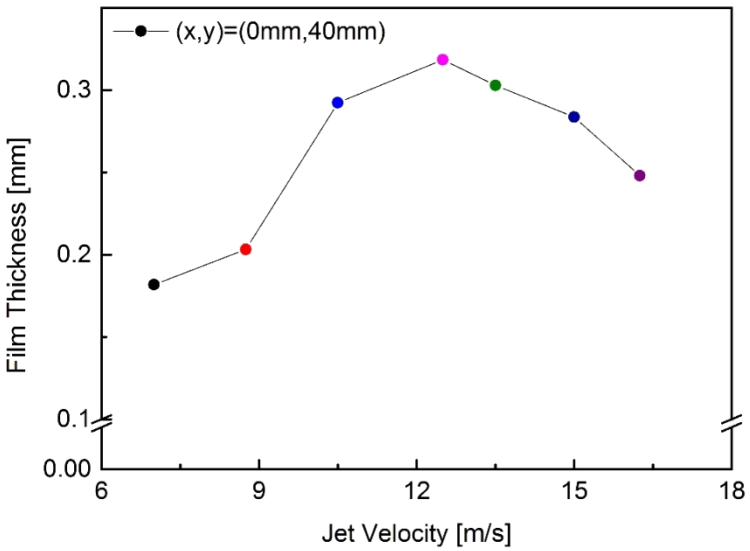

Figure 3.15 Film thickness at the (x=0mm, y=40mm) depending on jet speed

Figure 3.15 graph shows that the film thickness increases as the jet velocity increases in the early stage. However, it can be seen that the liquid film thickness decreases again after the injection speed reaches about 12 m / s. This result means that the higher the injection velocity, the larger the injection flow rate, but the larger the injection flow rate, the larger the thickness of the liquid film does not mean. The reason is that if the jetted fluid has a higher collision momentum than the surface tension formed on the liquid film, the liquid film thickness becomes thinner because the flow rate of the liquid droplets becomes larger. That is, to form a thick liquid film thickness, it meant that the injection pressure difference had to be optimized appropriately.

Chapter 4. CONCLUSION

Liquid film characteristics of jet impingement between slit injector and wall depending on angle, jet velocity, and distance have been studied. To analyze the experimental results, qualitative and quantitative results were compared and analyzed. The larger the injection angle under various conditions, the wider the liquid film area and the thinner liquid film thickness of the main stream. The larger the injection speed, the greater the perturbation of the liquid film and the greater the liquid film thickness of the main stream. Finally, it was analyzed that the injection distance does not have a large effect on the liquid film formation characteristics.

In summary, it was concluded that the liquid film characteristics of the collision injection between the slit injector and the wall have a large effect on the injection angle and injection speed, but the injection distance does not have a large effect. In addition, the hydraulic jump phenomenon has a great influence on whether the liquid film thickness in the axial direction becomes thicker or thinner toward the downstream side. Finally, to ensure that the main flow after collision is at the maximum liquid film thickness, we have to find an optimized

and appropriate injection flow rate.

If the stability factor is calculated to incorporate this thesis into film cooling studies, it will be of direct benefit to film cooling studies. In addition, if the ripple wave and perturbation are analyzed based on the FPCB to improve the liquid film thickness measuring device, a study on the dynamic characteristics will be possible.

References

[1] E. Kianpour, N. A. C. Sidik and M. A. Wahid, "Cylindrical and Row Trenched Cooling Holes with Alignment Angle of 90 Degree at Different Blowing Ratios," *CFD Letters,* 2013.

[2] A. G. Vorobyov, "Experimeantal-theoretical Model of Thermal Condition of Bi-propellant Small Liquid Rocket Engine Combustion Chamber, Working on Continuous Mode," *MAI,* 2010.

[3] D. Y. Bogacheva, "Modeling of Small Rocket Engine Internal Film Cooling by Gas-phased Ecological Clean Propellant Components," *MAI Ph. D. Thesis,* 2014.

[4] E. L. Knuth, "The Mechanics of Film Cooling - Part 1," *Journal of Jet Propulsion,* vol. 24, pp. 359-365, 1954.

[5] R. Arnold, D. I. Suslov and O. J. Haidn, "Experimental Investigation of Film Cooling with Tangential Slot Injection in a LOXCH4 Subscale Rocket Combustion Chamber," *JSASS Space Tech.,* vol. Vol 7, 2009.

[6] T. Inamura, H. Yanaoka, and T. Tomoda, "Prediction of Mean Droplet Size of Sprays Issued from Wall Impingement Injector," *AIAA Journal,* vol. 42, pp. 614-621, 2004.

[7] M. Damsohn and H. M. Prasser, "High-speed Liquid Film Sensor for Two-phase Flows with High Spatial Resolution Based on Electrical Conductance," *Flow Measurement and Instrumentation,* vol. 20, pp. 1-14, 2009.

[8] Y. S. Chudina, "Working Process in Small Size GOX/GCH4 Rocket Engine," *MAI,* 2014.

[9] H. M. Prasser, A. Bottger, and J. Zschau, "A new electrode-mesh

tomograph for gas–liquid flows," *Flow Measurement and Instrumentation*, pp. 111-119, 1998.

[10] NASA, "Liquid rocket engine self-cooled combustion chambers NASA SP-8124," 1977.

[11] M. Kondoh and M. Tsubouchi, "Liquid-sheet jets for terahertz spectroscopy," *Opt Express*, vol. 22, pp. 14135-47, Jun 16 2014.

[12] D. Ito, P. Papadopoulos, and H. M. Prasser, "Liquid film dynamics of two-phase annular flow in square and tight lattice subchannels," *Nuclear Engineering and Design*, vol. 300, pp. 467-474, 2016.

초 록

벽에 슬릿 인젝터로 물을 분사하여 형성된 액막을 실험적 접근으로 정성적 결과와 정량적 결과를 비교 분석했다. 로켓 막냉각 연구에서 열전달적 관점의 분석은 많지만, 수력학적 관점의 분석은 상대적으로 적다. 그러므로, 다양한 실험 조건에서 액막 두께 분포를 측정하여 액막의 특성을 분석하고자 했다. 먼저, 분포를 정성적으로 분석하기 위해 백라이트 이미지 기법을 이용하여 이미지를 취득했다. 다음으로는, 정량적 분석을 위해 전기 전도 방법을 기반으로 한 액막 두께 측정 장치를 직접 개발하여 액막 특성을 분석했다. 분사각 (15°, 30°, 45°), 분사 속도 (7m/s, 10.5m/s, 13.5m/s), 그리고 분사 거리 (45mm, 55mm, 65mm)를 실험 조건으로 선정했고, 그에 따른 정 특성 반응을 분석했다. 분사각이 커짐에 따라 주 흐름의 두께는 점차 얇아지는 것을 확인했고, 또한 최대 액막 두께의 위치가 상류 방향으로 이동하는 것을 관측했다. 분사 속도가 빨라짐에 따라서는 액막의 면적이 넓어지고, 액막의 섭동이 더 커지는 것을 관찰했다. 마지막으로

분사 거리는 형성된 액막에 큰 영향을 주지 못하는 것을 알 수 있었다. 실험 결과를 기반으로 도수 현상 또한 관측하였고, 도수 현상은 주 흐름의 액막 두께 분포에 큰 영향을 미치는 것을 파악했다. 이 연구의 결과를 막 냉각을 이용하는 추력기 또는 로켓 엔진 개발에 적용하여 보다 진보된 막 냉각 분석을 할 수 있을 것이다.

주요어: 슬릿 인젝터, 액막 두께, 고속 와이어-메시 방법, 도수 현상
학 번: 2016-20751